Volume 6
Number 18
21 September 2025
Pages 6197–6598

Materials Advances

rsc.li/materials-advances

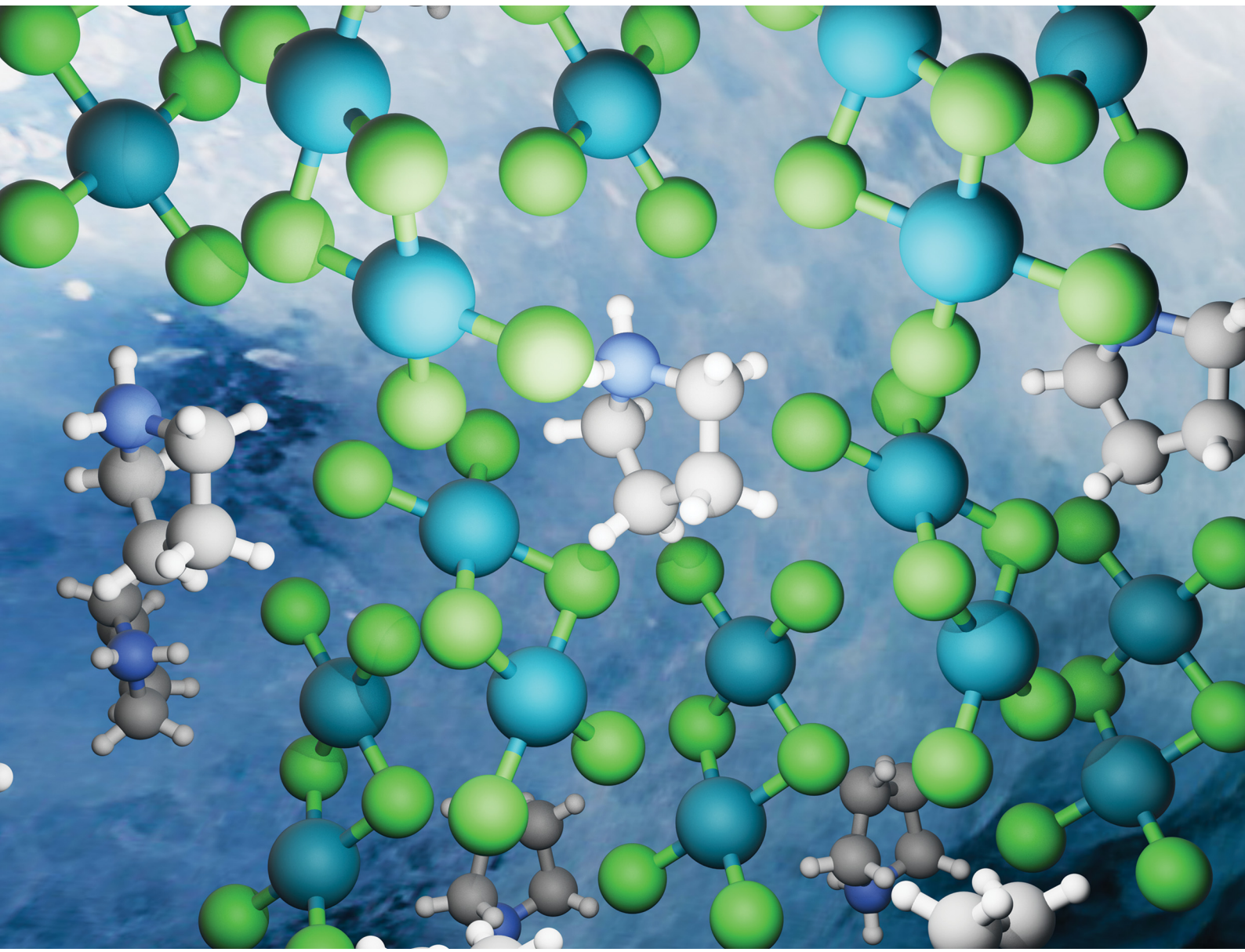

ISSN 2633-5409

ROYAL SOCIETY OF CHEMISTRY

PAPER
Daniel B. Straus *et al.*
The emergence of intrinsic chirality in copper and palladium chloride materials

Materials Advances

ROYAL SOCIETY OF CHEMISTRY

PAPER

View Article Online
View Journal | View Issue

Cite this: *Mater. Adv.*, 2025, **6**, 6262

The emergence of intrinsic chirality in copper and palladium chloride materials†

Zheng Zhang,[a] Santu Biswas,[b] Matthew M. Montemore [b] and Daniel B. Straus *[a]

In most chiral organic–inorganic hybrid metal halides, chirality is extrinsically introduced by chiral organic cations because the inorganic framework is otherwise achiral. However, there are a few hybrid metal halides where chirality emerges spontaneously, *i.e.* in the absence of chiral molecules. Yet, the mechanisms that cause this intrinsic chirality to emerge are unclear. In this work, we report the discovery and investigation of the intrinsically chiral material pyrrolidinium palladium chloride ($(C_4H_{10}N)PdCl_3$), which consists of bent edge-sharing square-planar palladium chloride dimers separated by $[C_4H_{10}N]^+$ cations. Its crystal structure indicates that hydrogen bonding interactions between N-bound hydrogens and Cl^- anions induce chirality, and this hypothesis is supported by the achirality of the all-inorganic material $CsPdCl_3$ as well as our density functional theory calculations. The situation is reversed for octahedrally coordinated copper(II) chlorides, where previous reports show that $(C_4H_{10}N)CuCl_3$ is achiral while $CsCuCl_3$ exhibits intrinsic chirality. This reversal is caused by the electronic degeneracy in octahedral Cu^{2+}. In $CsCuCl_3$, cooperative Jahn–Teller distortions cause Cu^{2+} ions to move off-center within their octahedra, inducing chirality, while hydrogen bonding interactions with $(C_4H_{10}N)CuCl_3$ break symmetry, so the cooperative chiral distortion no longer occurs. Although the source of intrinsic chirality is usually unclear, our findings show that hydrogen bonding interactions can cause intrinsic chirality to emerge in organic–inorganic hybrid materials. They also highlight the importance of the metal's electron configuration and metal-halide coordination geometry on the emergence of intrinsic chirality, thereby providing guidance for the targeted synthesis of intrinsically chiral organic–inorganic hybrid materials.

Received 26th June 2025,
Accepted 28th June 2025

DOI: 10.1039/d5ma00682a

rsc.li/materials-advances

Introduction

Halide perovskites and derivative metal halide materials have shown great promise for applications such as ionizing radiation detection, solar energy harvesting, circularly polarized light (CPL) detection, and spin-related optoelectronics.[1–4] For CPL and spin optoelectronic applications, a material is required to be chiral so that right- and left-handed polarized light can be differentiated and/or spin-polarized charge transport can be achieved.[2,4] Nearly all metal-halide frameworks are, by themselves, achiral.[5,6] In these instances, chirality must be extrinsically induced into the metal-halide framework, which is typically achieved by incorporating an enantiomerically pure chiral organic ligand into the metal halide.[7,8] Many extrinsically chiral organic–inorganic metal halide materials have been synthesized, including the copper-based $(R/S\text{-ClMBA})_2CuCl_4$, $(R/S\text{-NA})_2CuBr_4$, and $(R\text{-MBA})CuBr_2$; and the lead-based $(R\text{-MBA})_2PbI_4$, $(R/S\text{-MBnP})PbI_3$, and $(R/S\text{-3AEP})Pb_2I_6$ (where ClMBA = 4-(chloromethyl)-benzylammonium, NA = nipecotic acid, MBA = *a*-methylbenzylammonium, 3AEP = 3-(1-aminoethyl)pyridin-1-ium, MBnP = methylbenzylpyridinium).[7–13]

When an organic–inorganic hybrid metal halide material is synthesized with a racemic mixture of chiral cations, the resulting structure is typically achiral because it incorporates equal numbers of left- and right-handed molecules, so there is no net handed distortion.[7] On some occasions, spontaneous resolution occurs, resulting in the formation of a mixture of left- and right-handed crystals that respectively contain exclusively left- or right-handed organic molecules.[14]

In the absence of chiral molecules, it is possible for intrinsic chirality to emerge in crystalline materials when the arrangement of atoms and/or molecules within a crystal is chiral, even though the atomic, ionic, or molecular building blocks are themselves achiral.[15] In a single crystallization of an intrinsically chiral material, both left- and right-handed crystals can form as there are no chiral centers that force the formation of

[a] *Department of Chemistry, Tulane University, New Orleans, Louisiana 70118, USA. E-mail: dstraus@tulane.edu*
[b] *Department of Chemical and Biomolecular Engineering, Tulane University, New Orleans, Louisiana 70118, USA*

† Electronic supplementary information (ESI) available: Experimental methods; additional figures and tables; crystal structures. CCDC 2434800 and 2434814. For ESI and crystallographic data in CIF or other electronic format see DOI: https://doi.org/10.1039/d5ma00682a

crystals of a single handedness.[15,16] Intrinsically chiral crystals occur in covalent inorganic materials such as α- and β-quartz (SiO_2),[17] in ionic inorganic materials such as $NaClO_3$ and the metal halide $CsCuCl_3$,[15,18–21] in molecular solids such as *o*-terphenyl and $C_{60}(SnI_4)_2$,[22–24] and in organic–inorganic hybrid materials such as $(TMA)CuCl_3$ (TMA = tetramethylammonium).[25,26] However, it is not currently possible to predictively synthesize new intrinsically chiral materials.

Several phenomena have been hypothesized to be possible sources of intrinsic chirality. One such phenomenon is the cooperative Jahn–Teller effect,[27,28] which can be observed in the all-inorganic chiral hexagonal perovskite $CsCuCl_3$ as well as the isostructural organic–inorganic hybrid material $(TMA)CuCl_3$. Typical hexagonal perovskites consist of negatively charged one-dimensional (1D) chains of face-sharing octahedra separated from one another by cations, and nearly all hexagonal perovskites that do not contain chiral organic molecules are achiral. In contrast, $CsCuCl_3$ is chiral, crystallizing in the enantiomorphic hexagonal space groups $P6_122$ and $P6_522$. Chirality in $CsCuCl_3$ originates from cooperative Jahn–Teller distortions caused by the electronic degeneracy in and point symmetry of octahedrally-coordinated Cu^{2+} that cause each Cu^{2+} ion to move off-center in its octahedron, resulting in the formation of a helical structure within each one-dimensional chain.[29,30] The same phenomenon occurs in $(TMA)CuCl_3$,[26] which crystallizes in the $P2_1$ Sohncke space group, which supports chiral structures.

For achiral organic molecules, three factors are known to influence the formation of chiral crystal structures: hindered rotation about bonds, helical packing arrangements, and head-to-head stacking in columnar arrangements.[22] Quasi-planar aromatic and/or floppy achiral molecules can form chiral crystal structures as these molecular shapes allow for many possible helical packing arrangements within crystals. However, high-symmetry achiral molecules can also crystallize into chiral crystal structures as demonstrated by the chiral crystallization of icosahedral C_{60} and tetrahedral SnI_4,[23] indicating that much remains to be discovered about what induces the formation of intrinsically chiral materials.

In this work, we report that hydrogen bonding interactions cause chirality to emerge in the organic–inorganic hybrid material pyrrolidinium palladium chloride ($[C_4H_{10}N]PdCl_3$), which does not contain chiral molecules. In this structure, isolated Pd_2Cl_6 units consisting of bent dimers of edge-sharing Pd–Cl square planar motifs are separated from one another by $[C_4H_{10}N]^+$ cations. Its crystal structure reveals that hydrogen bonding interactions between N-bound hydrogens on the $[C_4H_{10}N]^+$ cation and Cl^- anions induce the formation of a chiral structure, and this conclusion is supported by density functional theory (DFT) calculations. In contrast, the all-inorganic material $CsPdCl_3$ is achiral, likely because symmetry-breaking hydrogen bonding interactions are not possible when $[C_4H_{10}N]^+$ is replaced by Cs^+. We also investigate fundamental differences in the emergence of intrinsic chirality in palladium(II) and copper(II) chlorides. Unlike the intrinsically chiral $(C_4H_{10}N)PdCl_3$, $(C_4H_{10}N)CuCl_3$ is an achiral one-dimensional hexagonal perovskite, in contrast to intrinsically chiral $CsCuCl_3$ and $(TMA)CuCl_3$, all of which are previously reported. Hydrogen bonding between N-bound hydrogens on the $[C_4H_{10}N]^+$ cations and Cl^- anions breaks symmetry, thereby lowering the point symmetry of Cu^{2+} such that the cooperative Jahn–Teller distortions that induce chirality in $CsCuCl_3$ and $TMACuCl_3$ no longer occur. Our findings demonstrate that hydrogen bonding interactions can be used to induce the formation of intrinsically chiral organic–inorganic hybrid materials. They also highlight how the interplay of the metal's electronic configuration, point symmetry, and coordination geometry with the achiral cation's structure affect the emergence of intrinsic chirality, providing principles that can be used for the design and synthesis of new intrinsically chiral materials.

Results and discussion

Crystals of $(C_4H_{10}N)PdCl_3$ are grown in solution through the slow evaporation of concentrated hydrochloric acid and characterized using single-crystal X-ray diffraction (SCXRD) measurements (see ESI†). The crystal structure of intrinsically chiral $(C_4H_{10}N)PdCl_3$ is shown in Fig. 1 and Fig. S1 (ESI†), consisting of bent inorganic $[Pd_2Cl_6]^{2-}$ dimers separated by $[C_4H_{10}N]^+$ organic cations (Fig. 1a). At room temperature, $(C_4H_{10}N)PdCl_3$ crystallizes in the orthorhombic $P2_12_12_1$ (#19) Sohncke space

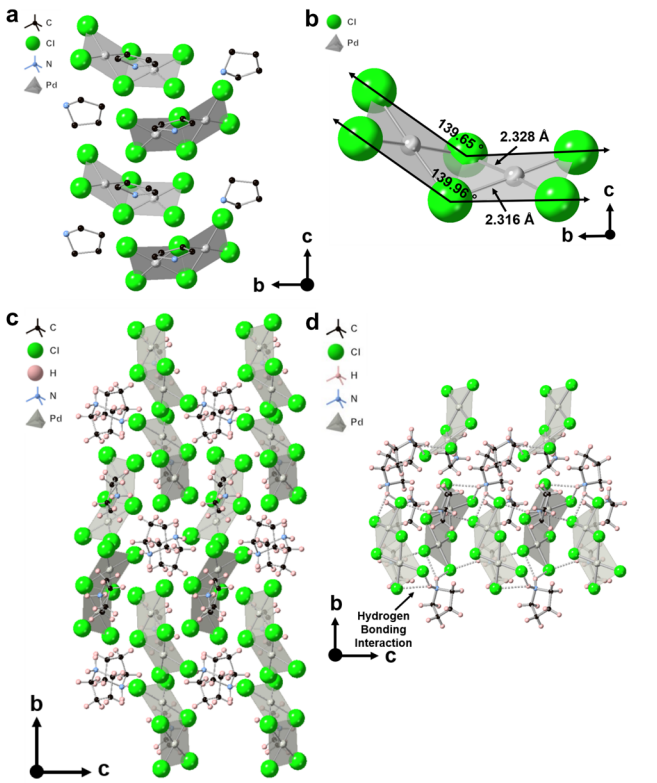

Fig. 1 (a) Single crystal structure of $(C_4H_{10}N)PdCl_3$ viewed down *a*. H atoms omitted for clarity. (b) A single $[Pd_2Cl_6]^{2-}$ dimer to show the bond distance and bond angle within the dimer. (c) Helical packing arrangement of the crystal structure viewed down *a*, with (d) hydrogen bonding interactions shown in dashed lines.

Table 1 Crystallographic collection and structural refinement parameters of $(C_4H_{10}N)PdCl_3$

Formula	$(C_4H_{10}N)PdCl_3$
Formula weight (g mol^{-1})	284.88
Temperature (K)	300
Wavelength (Å)	1.54178
Crystal system	Orthorhombic
Space group	$P2_12_12_1$ (#19)
Z	8
Unit cell parameters (Å)	a = 11.4392(2) b = 19.7418(4) c = 8.0453(2)
Volume (Å^3)	1816.87(7)
Density (g cm^{-3})	2.083
Absorption coefficient (μ) (mm^{-1})	23.979
$\theta_{min} - \theta_{max}$ (°)	8.958 to 148.38
Reflections collected	23 053
Independent reflections	3671 [R_{int} = 0.0340, R_{sigma} = 0.0246]
Ra indices ($I > 2\sigma(I)$)	R_1 = 0.0219 wR_2 = 0.0563
Goodness-of-fit on F^2	1.051
Largest diff. peak/hole (e$^-$ Å^{-3})	0.42/−0.43
Flack parameter	0.020(7)

group, which supports chiral structures, with unit cell parameters a = 11.4392(2), b = 19.7418(4), and c = 8.0453(2) Å (Table 1). $(C_4H_{10}N)PdCl_3$ is intrinsically chiral, and our structure has a Flack parameter of 0.020(7), indicating that we resolved the absolute configuration (*i.e.*, handedness) of the studied crystal.[15] In a single $[Pd_2Cl_6]^{2-}$ dimer (Fig. 1b), the Cl–Cl–Cl angles are 139.96(7)° and 139.65(7)°. Within the $[Pd_2Cl_6]^{2-}$ dimer, the Pd–Cl bond distance is measured to be ~2.3 Å, which is slightly shorter than the sum of the Shannon ionic radii of 2.45 Å for four-coordinate square-planar Pd^{2+} and six-coordinate Cl^- ions;[31] we use the six-coordinate Cl^- ionic radius because Shannon's table does not include ionic radii for one- or two-coordinate Cl^- as found in $(C_4H_{10}N)PdCl_3$. The measured Pd–Cl bond distance here in $(C_4H_{10}N)PdCl_3$ is similar to the Pd–Cl bond distance in other four-coordinate palladium chlorides such as $(NH_4)_2PdCl_4$ (2.345 Å, ref. 32), $CsPdCl_3$ (2.234 Å, ref. 33), K_2PdCl_4 (2.318 Å, ref. 34), and chiral (*R*/*S*-$C_5H_{14}N_2)PdCl_4$ (2.311 Å, ref. 35). The powder X-ray diffraction (PXRD) pattern of our bulk material (Fig. S2, ESI†) matches the simulated pattern obtained from our single-crystal structure, demonstrating that our material is phase-pure. $(C_4H_{10}N)PdCl_3$ is air-stable for at least eight weeks as the PXRD pattern does not change (Fig. S3, ESI†).

The unexpected emergence of intrinsic chirality in $(C_4H_{10}N)PdCl_3$ encouraged us to further investigate the origin of its chirality, especially given the simplicity of the $[C_4H_{10}N]^+$ organic cation. Based on our examination of the Cambridge Structural Database (CSD),[36] all organic–inorganic hybrid materials containing $[Pd_2Cl_6]^{2-}$ moieties are achiral (excluding structures that contain chiral cations) including $(C_8H_{20}N)_2[Pd_2Cl_6]$,[37] $(C_{16}H_{20}N)_2[Pd_2Cl_6]$,[38] $(C_{19}H_{25}N_2)_2[Pd_2Cl_6]$,[39] $(C_{30}H_{24}N_6Ru)_2[Pd_2Cl_6]_2{\cdot}H_2O$,[40] $(C_{21}H_{28}P)_2[Pd_2Cl_6]$,[41] $(C_{35}H_{25}ClN_5Pd)_2[Pd_2Cl_6]$,[42] $(H_3O)_2(C_{50}H_{60}N_{20}O_{10})[Pd_2Cl_6]{\cdot}3H_2O$,[43] $(C_{45}H_{42}ClOP_2PtS)_2[Pd_2Cl_6]{\cdot}4(CHCl_3)$.[44] In addition, the all-inorganic material $CsPdCl_3$,[45] which also contains $[Pd_2Cl_6]^{2-}$ dimers, is also achiral. A closer examination of the crystal structure of $(C_4H_{10}N)PdCl_3$ down the *a* axis (Fig. 1c) shows that the $[Pd_2Cl_6]^{2-}$ dimers exhibit a helical packing arrangement. Hydrogen bonding interactions between the N bound hydrogens (which have refined coordinates in our structure) and Cl^- anions in $[Pd_2Cl_6]^{2-}$ dimers (Fig. 1d) appear to be the driving force that induces the helical packing arrangement in $(C_4H_{10}N)PdCl_3$. In addition, hydrogen bonding interactions induce bending in $[Pd_2Cl_6]^{2-}$ dimers; most structures in the CSD contain planar $[Pd_2Cl_6]^{2-}$ dimers, and the structures containing bent $[Pd_2Cl_6]^{2-}$ dimers exhibit strong hydrogen bonding interactions. Notably, both $CsPdCl_3$ and $(C_8H_{20}N)_2[Pd_2Cl_6]$ ($[C_8H_{20}N]^+$ = tetraethylammonium) are achiral, contain planar $[Pd_2Cl_6]^{2-}$ dimers, and do not exhibit significant hydrogen bonding interactions.[37,45]

To test our hypothesis that hydrogen bonding interactions between N-bound H atoms and nearby Cl atoms are the source of chirality in $(C_4H_{10}N)PdCl_3$, we use DFT calculations on our experimental structure as well as on model structures. Overall, we find that the DFT calculations agree well with the experimental results; for example, DFT accurately reproduces the lattice constants and the presence of chirality in $(C_4H_{10}N)PdCl_3$. We first perform DFT calculations on $[Pd_2Cl_6]^{2-}$ dimers alone without any cations present to understand the role of the cation in determining whether the $[Pd_2Cl_6]^{2-}$ dimers are planar or bent. We start by removing the $[C_4H_{10}N]^+$ organic ligand from the obtained experimental crystal structure and add two electrons and an equivalent positive uniform background charge to compensate for the removal of the cation (Fig. 2a). The $[Pd_2Cl_6]^{2-}$ dimers remain bent after relaxing the structure. Similarly, starting with a nearly planar $[Pd_2Cl_6]^{2-}$ dimer configuration, $[Pd_2Cl_6]^{2-}$ remains nearly planar with a bending angle of 174.02° (Fig. 2b). The two configurations are very similar in energy, with the bent configuration just 3 meV more stable. Because the energy difference between the two structures is so small, it is likely that interactions between the cation and $[Pd_2Cl_6]^{2-}$ dimers are responsible for determining whether $[Pd_2Cl_6]^{2-}$ dimers are planar or bent. We next introduce the $[C_4H_{10}N]^+$ cation into a model structure with planar $[Pd_2Cl_6]^{2-}$ dimers and find that the dimers spontaneously relax to the bent

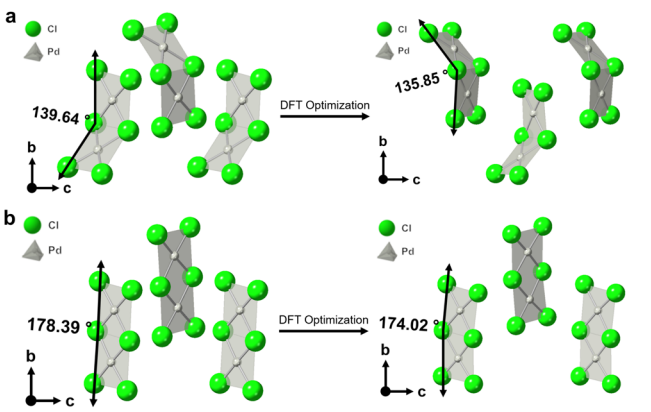

Fig. 2 DFT optimization results for (a) bent $[Pd_2Cl_6]^{2-}$ dimers and (b) linear $[Pd_2Cl_6]^{2-}$ dimers with no organic cation and extra electrons added to maintain the charge.

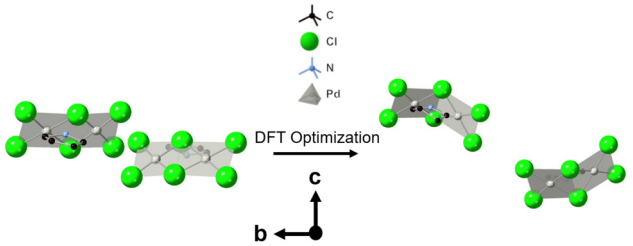

Fig. 3 DFT geometry optimization of planar $[Pd_2Cl_6]^{2-}$ dimers in the presence of $[C_4H_{10}N]^+$ cations. H atoms omitted for clarity.

configuration during DFT optimization (Fig. 3). Thus, the $[C_4H_{10}N]^+$ cation appears to cause the observed bending for the $[Pd_2Cl_6]^{2-}$ dimers. To further test the role of hydrogen bonding, we next perform additional calculations to attempt to reduce or modify the hydrogen bonding interactions by rotating the organic cation in the presence of both bent and planar $[Pd_2Cl_6]^{2-}$ dimers (Fig. S5, ESI†). These results confirm that hydrogen bonding interactions between N-bound H atoms and Cl^- cations are energetically favorable and support the conclusion that hydrogen bonding interactions are responsible for the arrangement of the organic $[C_4H_{10}N]^+$ cation and bent $[Pd_2Cl_6]^{2-}$ dimer.

Lastly, we replace Cs^+ with $[C_4H_{10}N]^+$ in achiral $CsPdCl_3$[46] and relax the structure to see if a chiral structure forms (Fig. 4a and b). We note that the model input structure we created (Fig. 4b) is achiral with 100% certainty according to the NEWSYM test in PLATON.[47] However, the DFT-optimized structure (Fig. 4c) contains bent $[Pd_2Cl_6]^{2-}$ dimers and is chiral with 100% probability according to the NEWSYM test. The emergence of chirality once Cs^+ is replaced with $[C_4H_{10}N]^+$ supports our hypothesis that hydrogen bonding interactions are responsible for inducing intrinsic chirality in $(C_4H_{10}N)PdCl_3$, and the presence of bent $[Pd_2Cl_6]^{2-}$ dimers is again attributed to hydrogen bonding interactions between the organic $[C_4H_{10}N]^+$ cation and Cl^- anions in the inorganic metal-halide $[Pd_2Cl_6]^{2-}$ framework.

In agreement with previous work, we find that the presence of $[C_4H_{10}N]^+$ does not guarantee the emergence of a chiral structure for metal cations other than Pd^{2+}. In addition to chiral $(C_4H_{10}N)PdCl_3$, we also synthesized the known material $(C_4H_{10}N)CuCl_3$.[48] $(C_4H_{10}N)CuCl_3$ is an achiral hexagonal perovskite that consists of 1D chains of face-sharing Cu–Cl octahedra, separated from one another by $[C_4H_{10}N]^+$ cations (Fig. 5a, b and Fig. S6, ESI†). At room temperature, $(C_4H_{10}N)CuCl_3$ crystallizes in the centrosymmetric monoclinic space group $P2_1/n$ (#14) with unit cell parameters a = 9.3503(12) Å, b = 6.5136(8) Å, c = 14.1378(18) Å, and β = 102.931(3)° (see Table S1 for detailed refinement parameters, ESI†). In contrast, $CsCuCl_3$ (Fig. 5c and d) and $(TMA)CuCl_3$[26,49] form intrinsically chiral hexagonal perovskites because cooperative Jahn–Teller distortions cause the Cu^{2+} cations to move off-center within their octahedra (Fig. 5d), forming a helical structure in each 1D

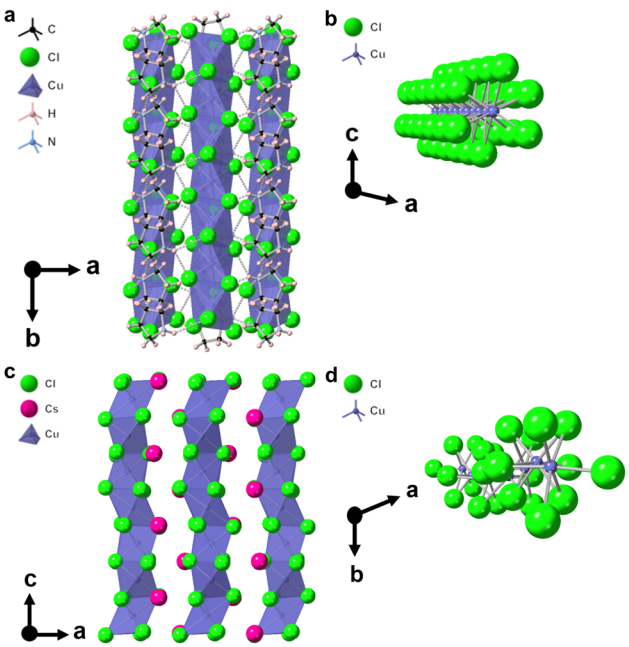

Fig. 5 (a) Crystal structure of achiral $(C_4H_{10}N)CuCl_3$, with hydrogen bonds shown as dashed lines, and (b) alternate view of its 1D Cu–Cl chain. (c) Crystal structure of chiral $CsCuCl_3$ and (d) alternate view of its 1D Cu–Cl chain.

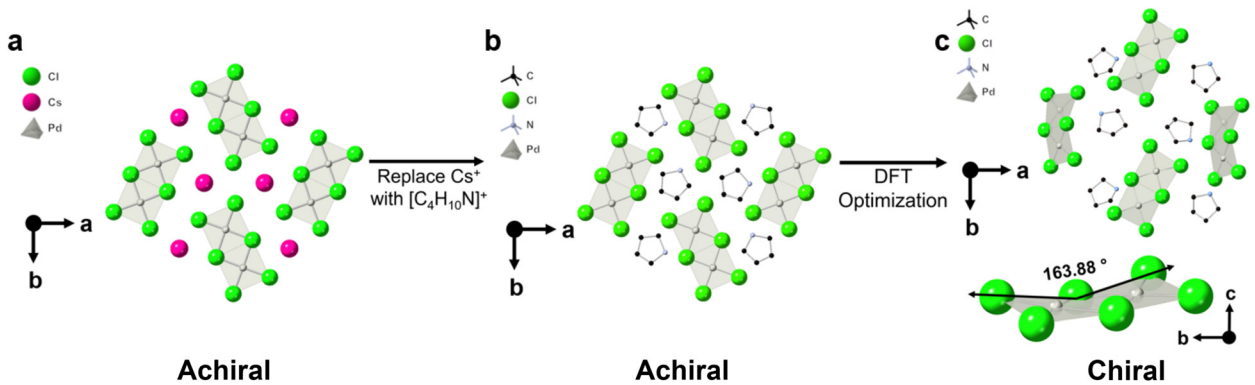

Fig. 4 (a) Crystal structure of achiral $CsPdCl_3$. (b) Crystal structure after replacing Cs^+ with $[C_4H_{10}N]^+$ in $CsPdCl_3$. (c) DFT optimized chiral structure after replacing Cs^+ with $[C_4H_{10}N]^+$ in $CsPdCl_3$. H atoms omitted for clarity in (b) and (c).

chain.[30] In $(C_4H_{10}N)CuCl_3$, hydrogen bonding interactions between N-bound hydrogens on the $[C_4H_{10}N]^+$ cation and Cl^- anions change the point symmetry of the Cu^{2+} cation by causing some Cl^- anions to become symmetry inequivalent, so the cooperative helical Jahn–Teller distortions that cause $CsCuCl_3$ and $(TMA)CuCl_3$ to be intrinsically chiral no longer exist. Therefore, hydrogen bonding interactions serve to make intrinsically chiral Cu^{2+} hexagonal perovskites achiral, demonstrating the interplay between the metal's electron configuration, its coordination geometry, and hydrogen bonding interactions on the formation of intrinsically chiral materials. When cooperative Jahn–Teller distortions are not present, we hypothesize that hydrogen bonding interactions are likely to induce chirality; additional work is required to confirm this hypothesis. In materials where cooperative Jahn–Teller distortions are present, hydrogen bonding interactions will change the local symmetry and the nature of the cooperative distortions, causing intrinsically chiral materials to become achiral.

Conclusions

In summary, we report the intrinsically chiral metal halide $(C_4H_{10}N)PdCl_3$ that contains no chiral molecules. Structural analysis and DFT calculations show that chirality emerges from a helical packing arrangement induced by hydrogen bonding interactions between the organic and inorganic components. In contrast, other palladium(II) chlorides such as $CsPdCl_3$ and $(C_8H_{20}N)PdCl_3$ that do not contain chiral molecules are achiral because they do not exhibit hydrogen bonding interactions that induce a similar helical packing arrangement. Copper(II) chlorides behave quite differently. $CsCuCl_3$ and $(TMA)CuCl_3$ are chiral because cooperative Jahn–Teller distortions cause Cu^{2+} to move off-center within its octahedron and form a helical structure in each 1D chain, whereas hydrogen bonding interactions in $(C_4H_{10}N)CuCl_3$ cause it to be achiral as these interactions stop the chirality-inducing cooperative Jahn–Teller distortions from occurring. Our findings demonstrate that organic–inorganic hydrogen-bonding interactions can induce chirality in achiral metal halide materials and reveal the interplay between hydrogen bonding interactions with the metal's electronic configuration, coordination geometry, and point symmetry in determining whether a material will be intrinsically chiral.

Conflicts of interest

There are no conflicts to declare.

Data availability

The data supporting this article, including experimental details and supplementary figures, have been included as part of the ESI.† Crystallographic data have been deposited at the Cambridge Crystallographic Data Centre under deposition numbers 2434800 and 2434814.

Acknowledgements

Primary support is provided by the Louisiana Board of Regents under contract LEQSF(2024-27)-RD-A-28. Computational work is primarily supported by the National Science Foundation through grant CBET-2340356 and uses high performance computing resources and services provided by Technology Services at Tulane University. The authors acknowledge additional financial support from Tulane University and thank Dr Xiaodong Zhang for assistance with single crystal X-ray diffraction measurements.

References

1 N. T. P. Hartono, H. Köbler, P. Graniero, M. Khenkin, R. Schlatmann, C. Ulbrich and A. Abate, Stability Follows Efficiency Based on the Analysis of a Large Perovskite Solar Cells Ageing Dataset, *Nat. Commun.*, 2023, **14**(1), 1–7.
2 T. Liu, W. Shi, W. Tang, Z. Liu, B. C. Schroeder, O. Fenwick and M. J. Fuchter, High Responsivity Circular Polarized Light Detectors Based on Quasi Two-Dimensional Chiral Perovskite Films, *ACS Nano*, 2022, **16**(2), 2682–2689.
3 H. Hu, G. Niu, Z. Zheng, L. Xu, L. Liu and J. Tang, Perovskite Semiconductors for Ionizing Radiation Detection, *EcoMat*, 2022, **4**(6), e12258.
4 Q. Wang, Y. Lu, R. L. He, R. Chen, L. Qiao, F. Pan, Z. Yang and C. Song, Spin Selectivity in Chiral Hybrid Cobalt Halide Films with Ultrasmooth Surface, *Small Methods*, 2022, **6**(12), 2201048.
5 J. A. McNulty and P. Lightfoot, Unprecedented Tin Iodide Perovskite-like Structures Featuring Ordering of Organic Moieties, *Chem. Commun.*, 2020, **56**(33), 4543–4546.
6 D. H. Fabini, K. Honasoge, A. Cohen, S. Bette, K. M. McCall, C. C. Stoumpos, S. Klenner, M. Zipkat, L. P. Hoang, J. Nuss, R. K. Kremer, M. G. Kanatzidis, O. Yaffe, S. Kaiser and B. V. Lotsch, Noncollinear Electric Dipoles in a Polar Chiral Phase of $CsSnBr_3$ Perovskite, *J. Am. Chem. Soc.*, 2024, **146**(23), 15701–15717.
7 A. Dibenedetto, C. Coccia, M. Boiocchi, M. Moroni, C. Milanese and L. Malavasi, Synthesis and Characterization of Cu-Containing Chiral Metal Halides and Role of Halogenation of the Organic Ligand, *J. Phys. Chem. C*, 2024, **128**(11), 4803–4808.
8 X. Wang, Y. Wu, F. Gao and Y. Wang, Chiral Zero-Dimensional Hybrid Organic-Inorganic Metal Halides Based on Nipecotic Acid and Tetrabromocuprate, *New J. Chem.*, 2024, **51**(7), 3192–3198.
9 F. Ge, B. H. Li, P. Cheng, G. Li, Z. Ren, J. Xu and X. H. Bu, Chiral Hybrid Copper(I) Halides for High Efficiency Second Harmonic Generation with a Broadband Transparency Window, *Angew. Chem., Int. Ed.*, 2022, **61**(10), e202115024.
10 C. C. Fan, C. D. Liu, B. D. Liang, T. Y. Ju, W. Wang, M. L. Jin, C. Y. Chai and W. Zhang, Chiral Three-Dimensional Organic-Inorganic Lead Iodide Hybrid Semiconductors, *Chem. Sci.*, 2024, **15**(29), 11374–11381.
11 D. G. Billing and A. Lemmerer, Synthesis and Crystal Structures of Inorganic-Organic Hybrids Incorporating an

Aromatic Amine with a Chiral Functional Group, *CrystEngComm*, 2006, **8**(9), 686–695.

12 S. Ma, Y. K. Jung, J. Ahn, J. Kyhm, J. Tan, H. Lee, G. Jang, C. U. Lee, A. Walsh and J. Moon, Elucidating the Origin of Chiroptical Activity in Chiral 2D Perovskites through Nano-Confined Growth, *Nat. Commun.*, 2022, **13**(1), 1–10.

13 R. Wan, M. Yin, T. H. Wang, C. E. Moore and Y. Wu, Chiral Methylbenzylpyridinium-Based Organic-Inorganic Lead Halides for Water-Resistant Photoluminescence Materials, *Inorg. Chem.*, 2025, 64.

14 M. Gruselle, R. Thouvenot, B. Malézieux, C. Train, P. Gredin, T. V. Demeschik, L. L. Troitskaya and V. I. Sokolov, Enantioselective Self-Assembly of Bimetallic $[Mn^{II}(\Delta)\text{-}Cr^{III}(C_2O_4)_3]$- and $[Mn^{II}(\Lambda)\text{-}Cr^{III}(C_2O_4)_3]$-Layered Anionic Networks Templated by the Optically Active (Rp), *Chem. – Eur. J.*, 2004, **10**(19), 4763–4769.

15 H. D. Flack, Chiral and Achiral Crystal Structures, *Helv. Chim. Acta*, 2003, **86**(4), 905–921.

16 D. K. Kondepudi, R. J. Kaufman and N. Singh, Chiral Symmetry Breaking in Sodium Chlorate Crystallization, *Science*, 1990, **250**(4983), 975–976.

17 M. G. Tucker, D. A. Keen and M. T. Dove, A Detailed Structural Characterization of Quartz on Heating through the α–β Phase Transition, *Mineral. Mag.*, 2001, **65**(4), 489–507.

18 K. Adachi, M. Mekata and N. Aciiiwa, Helical Magnetic Structure in $CsCuCl_3$, *J. Phys. Soc. Jpn*, 1980, **49**(2), 545–553.

19 A. F. Wells, The Crystal Structure of $CsCuCl_3$ and the Crystal Chemistry of Complex Halides ABX_3, *J. Chem. Soc.*, 1947, **0**, 1662–1670.

20 A. W. Schlueter, R. A. Jacobson and R. E. Rundle, A Redetermination of the Crystal Structure of $CsCuCl_3$, *Inorg. Chem.*, 1966, **5**(2), 277–280.

21 A. Rogalev, J. Goulon, F. Wilhelm, K. A. Kozlovskaya, E. N. Ovchinnikova, L. V. Soboleva, A. F. Konstantinova and V. E. Dmitrienko, Investigation of X-Ray Natural Circular Dichroism in a $CsCuCl_3$ Single Crystal: Theory and Experiment, *Crystallogr. Rep.*, 2008, **53**(3), 384–390.

22 T. Matsuura and H. Koshima, Introduction to Chiral Crystallization of Achiral Organic Compounds: Spontaneous Generation of Chirality, *J. Photochem. Photobiol., C*, 2005, **6**(1), 7–24.

23 D. B. Straus and R. J. Cava, Self-Assembly of a Chiral Cubic Three-Connected Net from the High Symmetry Molecules C_{60} and SnI_4, *J. Am. Chem. Soc.*, 2020, **142**(30), 13155–13161.

24 D. B. Straus and R. J. Cava, Generalizing the Chiral Self-Assembly of Spheres and Tetrahedra to Non-Spherical and Polydisperse Molecules in $(C_{70})_x(C_{60})_{1-x}(SnI_4)_2$, *Nano Lett.*, 2021, **21**(11), 4753–4756.

25 X. B. Han, C. Y. Chai, M. L. Jin, C. C. Fan and W. Zhang, Quartz-Like Structure, Optical Activity, and High Stability in the First Chiral Cation-Coordinated Perovskite Semiconductor, *Adv. Opt. Mater.*, 2023, **11**(19), 2300580.

26 R. D. Willett, M. R. Bond, W. G. Haije, O. P. M. Soonieus and W. J. A. Maaskant, Crystal Structures of Three Phases of Tetramethylammonium Trichlorocuprate(II)(TMCuC), *Inorg. Chem.*, 1988, **27**(4), 614–620.

27 I. B. Bersuker, The Jahn-Teller Effect in Crystal Chemistry and Spectroscopy, *Coord. Chem. Rev.*, 1975, **14**(4), 357–412.

28 J. B. Goodenough, Jahn-Teller Phenomena in Solids, *Annu. Rev. Mater. Sci.*, 1998, **28**(1), 1–27.

29 H. Ueda, E. Skoropata, M. Burian, V. Ukleev, G. S. Perren, L. Leroy, J. Zaccaro and U. Staub, Conical Spin Order with Chiral Quadrupole Helix in $CsCuCl_3$, *Phys. Rev. B*, 2022, **105**(14), 144408.

30 T. Ogihara, A Theory of Cooperative Jahn-Teller Effect: Structural Phase Transition in $CsCuCl_3$, *J. Phys. Soc. Jpn*, 1995, **64**(11), 4221–4241.

31 R. D. Shannon, Revised Effective Ionic Radii and Systematic Studies of Interatomic Distances in Halides and Chalcogenides, *Acta Crystallogr., Sect. A*, 1976, **32**(5), 751–767.

32 R. G. Dickinson, The Crystal Structures of Potassium and Ammonium Chlorostannates, *J. Am. Chem. Soc.*, 1922, **44**(2), 276–288.

33 B. Schuepp and H.-L. Keller, ChemInform Abstract: $CsPdCl_3$—A Compound with Isolated $[Pd_2Cl_6]$ Groups and an Inorganic Cation, *ChemInform*, 2000, **31**, 2.

34 R. H. B. Mais, P. G. Owston and A. M. Wood, The Crystal Structure of K_2PtCl_4 and K_2PdCl_4 with Estimates of the Factors Affecting Accuracy, *Acta Crystallogr., Sect. B*, 1972, **28**(2), 393–399.

35 B. B. Salah, F. Hajlaoui, K. Karoui, N. Audebrand, T. Roisnel, S. Freslon, N. Zouari and F. Jomni, Exploration of New Chiral Hybrid Semiconducting Palladium Halide Complexes: [(R)/(S)-2-Methylpiperazinediium]$PdCl_4$, *Mater. Res. Bull.*, 2023, **164**, 112251.

36 C. R. Groom, I. J. Bruno, M. P. Lightfoot and S. C. Ward, The Cambridge Structural Database, *Acta Crystallogr., Sect. B: Struct. Sci., Cryst. Eng. Mater.*, 2016, **72**(2), 171–179.

37 J. Fábry, M. Dušek, K. Fejfarová, R. Krupková, P. Vaněk and I. Němec, Two Phases of Bis(Tetraethyl-Ammonium) Di-μ-Chloro-Bis[Dichloro-Palladium(II)], *Acta Crystallogr., Sect. C: Cryst. Struct. Commun.*, 2004, **60**(9), m426–m430.

38 A. Peuronen, M. Lahtinen and J. Valkonen, The Conformational Polymorphism and Weak Interactions in Solid State Structures of Ten New Monomeric and Dimeric Substituted Dibenzyldimethylammonium Chloridopalladate Salts, *CrystEngComm*, 2009, **11**(11), 2344–2357.

39 B. Rogalewicz, T. Sierański, M. Szczesio, W. Maniukiewicz, A. Olczak, A. Korga-Plewko, M. Iwan, M. Michalczuk, B. Cury Camargo, J. Szczytko and A. Czylkowska, Physicochemical Characterization and Anticancer Activity of the New Imipramine Based Co(II), Pd(II) and Mn(II) Compounds, *Polyhedron*, 2023, **246**, 116638.

40 F. Pointillart, C. Train, F. Villain, C. C. Dit Moulin, P. Gredin, L. M. Chamoreau, M. Gruselle, G. Aullon, S. Alvarez and M. Verdaguer, Six-Fold Oxygen-Coordinated Triplet (S = 1) Palladium(II) Moieties Templated by Tris(Bipyridine)-Ruthenium(II) Ions, *J. Am. Chem. Soc.*, 2007, **129**(5), 1327–1334.

41 C. Jimeno, U. Christmann, E. C. Escudero-Adán, R. Vilar and M. A. Pericàs, Studies on the Amination of Aryl Chlorides with a Monoligated Palladium Catalyst: Kinetic Evidence for a Cooperative Mechanism, *Chem. – Eur. J.*, 2012, **18**(51), 16510–16516.
42 M. T. Jackson, N. C. Duncan, B. Rich, M. E. Jones, K. A. Brien, M. Spiegel, P. J. Farmer, K. K. Klausmeyer and C. M. Garner, Synthesis, Crystal Structures, and Characterization of the Complexes of the Bulky Ligand 2,6-Bis-(3′,5′-Diphenylpyrazolyl)Pyridine with Ruthenium, Rhodium, and Palladium, *Polyhedron*, 2018, **139**, 308–312.
43 R. X. Cheng, F. Y. Tian, Y. Q. Zhang and Z. Tao, Three Cucurbit[n]Uril-Based Supramolecular Frameworks Assembled by Planar Configuration $[PdnCLm]_2$-Anions, *Chin. J. Inorg. Chem.*, 2020, **36**(7), 1241–1248.
44 V. Subramaniyan, F. Tibika and Y. Tulchinsky, Effect of Internal Ligand Strain on Coordination Behavior of PSP Pincer Ligands, *Inorg. Chem.*, 2023, **62**(1), 123–136.
45 B. Schuepp and H.-L. Keller, ChemInform Abstract: $CsPdCl_3$—A Compound with Isolated $[Pd_2Cl_6]$ Groups and an Inorganic Cation, *ChemInform*, 2000, **31**, 2.
46 B. Schüpp and H. L. Keller, $CsPdCl_3$—A Compound with Isolated $[Pd_2Cl_6]$ Groups and an Inorganic Cation, *Z. Anorg. Allg. Chem.*, 1999, **625**(11), 1944–1950.
47 A. L. Spek, Structure Validation in Chemical Crystallography, *Acta Crystallogr., Sect. D: Biol. Crystallogr.*, 2009, **65**(2), 148–155.
48 D. M. Nilsen, G. V. Rubenacker, Z. Ping, J. E. Drumheller, R. D. Larsen and K. Emerson, Structure and Magnetic Moment of Pyrrolidinium Copper Trichloride, a Linear Ferromagnet, *Inorg. Chem.*, 1990, **29**(16), 2887–2888.
49 A. G. Christy, R. J. Angel, J. Haines and S. M. Clark, Crystal Structural Variation and Phase Transition in Caesium Trichlorocuprate at High Pressure, *J. Phys.: Condens. Matter*, 1994, **6**(17), 3125–3136.